Available online at www.sciencedirect.com
SCIENCE DIRECT
Journal of the European Ceramic Society 26 (2006) 711–718
www.elsevier.com/locate/jeurceramsoc

Effects of processing method and additive composition on microstructure and thermal conductivity of Si_3N_4 ceramics

Xinwen Zhu, You Zhou, Kiyoshi Hirao *

Advanced Manufacturing Research Institute, National Institute of Advanced Industrial Science and Technology (AIST), 2266-98 Shimo-Shidami, Nagoya 463-8560, Japan

Available online 11 August 2005

Abstract

A comparative investigation of sintered reaction-bonded silicon nitride (SRBSN) and sintered silicon nitride (SSN) was carried out by using two additive compositions of Y_2O_3–MgO and Yb_2O_3–MgO. The effects of additive composition on the processing, microstructure and thermal conductivity of both SRBSN and SSN materials were evaluated. It is shown that the replacement of Yb_2O_3 by Y_2O_3 has no significant effect on the densification, microstructure and thermal conductivity of SSN materials, but it has a large effect on the processing, microstructure and thermal conductivity of SRBSN materials. The replacement of Yb_2O_3 by Y_2O_3 results in highly bimodal microstructural development during post-sintering and this may be attributed to the formation of large rodlike β-nuclei during nitridation. Although the replacement of Yb_2O_3 by Y_2O_3 leads to the production of fully dense SRBSN materials, but it leads to a decrease in thermal conductivity, which is consistent with microstructural difference. More importantly, the present work implies that SRBSN materials with comparable thermal conductivity to SSN materials could be achieved.

Keywords: Reaction; Grain growth; Sintering; Thermal conductivity; Si_3N_4

1. Introduction

Silicon nitride (Si_3N_4) ceramics have a variety of structural applications such as engine component, heat exchanger, pump seal materials, ball bearings, cutting tools and so on, owing to the excellent mechanical properties at both room and elevated temperatures, good resistance to thermal shock and chemical attack, excellent creep resistance and very good tribological properties.[1] Also, Si_3N_4 is a potentially high thermal conductivity material with an intrinsic value of up to 200 $Wm^{-1} K^{-1}$.[2,3] The thermal conductivities of over 100 $Wm^{-1} K^{-1}$ have been achieved for β-Si_3N_4 ceramics. Due to the unique combination of high thermal conductivity and excellent mechanical properties, Si_3N_4 has been considered as a promising candidate for high performance substrates and heat sinks.[4]

Owing to the high degree of covalent bonding, in most cases, densification of Si_3N_4 requires sintering additives and proceeds via a liquid-phase sintering mechanism. With the aid of sintering additives such as MgO, Al_2O_3 and rare-earth oxides, dense Si_3N_4 ceramics can be produced from Si_3N_4 powder by hot-pressing (HPSN), sintering (SSN) and hot-isostatic pressing (HIPSN).[5] However, cost is always a major barrier to limit the widespread application of Si_3N_4 components. The desire for economically dense Si_3N_4 materials has led to the development of sintered reaction-bonded silicon nitride (SRBSN). With the introduction of sintering additives, the post-sintering allows the porous RBSN to reach complete densification. Owing to the combination of cheaper Si powder, machinability of RBSN body and lower sintering shrinkage, SRBSN offers a unique opportunity to reduce production cost of Si_3N_4 ceramics, compared with direct sintering of expensive Si_3N_4 powder.[5] Up to now, much work has been carried out concerning the processing and mechanical properties of SRBSN. Using 5 wt% Y_2O_3–2 wt% Al_2O_3 additives, some authors reported that SRBSN materials exhibited higher fracture strength than SSN materials, while the fracture toughness of the former is nearly equivalent to that of the latter.[6] Moreover, a fur-

* Corresponding author. Tel.: +81 52 736 7163; fax: +81 52 736 7405.
E-mail address: k-hirao@aist.go.jp (K. Hirao).

0955-2219/$ – see front matter © 2005 Elsevier Ltd. All rights reserved.
doi:10.1016/j.jeurceramsoc.2005.07.027

ther improvement in mechanical properties of SRBSN is feasible by optimising Si particle size and using β-Si_3N_4 seeds.[7]

Very recently, some attention has been paid to the thermal conductivity of SRBSN. The previous work reported that the Yb_2O_3–MgO and Y_2O_3–MgO compositions have an effect on the processing and thermal conductivity of SRBSN.[8] Using Y_2O_3–MgO as sintering additives, the SRBSN with thermal conductivity of $\sim$110 $Wm^{-1}K^{-1}$ has been produced.[9] Compared with SSN, the number of parameters influencing the microstructure and properties of SRBSN materials increases. In addition to the liquid-phase composition, the characteristics of RBSN (amount and particle size of β-phase and microstructure) would affect the post-sintering, microstructural evolution and properties of the final SRBSN. To well understand the role of processing method, a comparative investigation of the SSN and SRBSN materials is necessary. Therefore, the present work intends to study the effects of processing method on the microstructure and thermal conductivity of Si_3N_4 ceramics, using two different additive compositions—Yb_2O_3–MgO (YbM) and Y_2O_3–MgO (YM). A commercial α-Si_3N_4 powder and Si powder containing similar oxygen content were chosen to prepare SSN and SRBSN materials, respectively. Si green compacts were fully nitrided at 1400 °C under flow N_2. The Si_3N_4 powder and RBSN compacts are both densified by gas-pressure sintering at 1900 °C under 1 MPa N_2. Some factors affecting the microstructure and thermal conductivity of SSN and SRBSN were evaluated.

2. Experiment procedure

The starting materials used in this study were Si (oxygen content 1.28 wt%, d_{50} = 0.7 μm, Kojundo Chemical Laboratory Co. Ltd., Saitama, Japan), α-Si_3N_4 powder (SN E-10, oxygen content < 2 wt%, β < 5%, specific surface area of 9–13 m^2/g, UBE Industries Ltd., Yamaguchi, Japan), Yb_2O_3 (purity >99.9%, specific surface area of 19.3 m^2/g, Nihon Yttrium Co. Ltd., Tokyo, Japan) and MgO (1000A, UBE Industries Ltd., Japan). The compositions of Si compacts were determined based on the compositions after full nitridation as Si_3N_4:Yb_2O_3:MgO = 90:5:5 and Si_3N_4:Y_2O_3:MgO = 90:5:5 at molar ratios, designated as samples RYbM and RYM, respectively. The corresponding Si_3N_4-powder compacts were designated as samples SYbM and SYM, respectively.

All powder mixtures were mixed in a planetary mill for 1 h in a Si_3N_4 jar with Si_3N_4 balls, using methanol as a mixing medium. The slurry was dried using a rotary evaporator at a temperature of 60 °C, subsequently dried at 110 °C for at least 4 h in vacuum and sieved through 100 mesh screen. Two grams of powder mixture were uniaxially pressed in a 20 mm diameter stainless die and then cold isostatically pressed. The cold isostatic pressure used for Si compacts and Si_3N_4-powder compacts was 300 and 400 MPa, respectively. Based on the calculation by geometry method, samples RYbM and RYM have green densities of 59 and 57% of theoretical, respectively, and samples SYbM and SYM have green densities of 54 and 53% of theoretical, respectively. The Si compacts were nitrided in an alumina tube furnace with 1 L/min high purity nitrogen flow at 1400 °C for 8 h. The nitrided compacts and Si_3N_4-powder compacts were sintered inside a triple crucible arrangement which consisted of a double BN crucible and an outer graphite crucible in a graphite resistance furnace at 1900 °C for 6 h under a N_2 pressure of 1 MPa. A BN powder (GP grade, Denki Kagaku Kogyo Co., Japan) was used as powder bed.

The extent of nitridation was determined by the ratio of the observed weight gain and theoretical weight gain according to the reaction ($3Si \rightarrow Si_3N_4$). Linear shrinkage was determined by the apparent dimensional change of disk samples during nitridation and sintering. Weigh loss was determined by the apparent weight change of samples before and after sintering. Bulk density was measured by the Archimedes method using distilled water as an immersion medium. Theoretical density of sintered RBSN and Si_3N_4-powder compacts was estimated based on their designed compositions by the rule of mixture.

The phase analysis of the nitrided and sintered materials was conducted on the cross-sections of the bulk samples by using X-ray diffractometry (XRD) (Model RINT 2500, Rigaku Co., Tokyo, Japan, Cu Kα radiation, scanning range of 2θ = 10–70°, operating conditions of 40 kV and 100 mA). The quantitative analysis of α- and β-Si_3N_4 of the nitrided products was performed using the method described by Pigeon and Varma (scanning rate: 0.5° 2θ/min).[10] The fracture surfaces of the nitrided bodies were observed by scanning electron microscopy (SEM) (Model JSM–5600, JEOL, Tokyo, Japan). Cross-sections of sintered materials were polished with a 1 μm diamond slurry and subsequently plasma-etched in a CF_4 gas. The etched surfaces were observed by SEM.

Disk specimens with a dimension of 10 mm diameter and 2 mm thickness were prepared by grinding sintered materials. Thermal diffusivity was measured by the laser-flash method (Model TC-7000, ULVAC, Yokohama, Japan). Prior to measurement, the surfaces of the specimens were sputter-coated a 600 Å thick layer of gold to avoid direct transmission of the laser pulse, followed by a subsequent coating of colloidal graphite to enhance absorption of the flash energy. Thermal conductivity (k) was calculated according to the equation:

$$k = \rho C_p \alpha \quad (1)$$

where ρ, C_p, and α are bulk density, specific heat, and thermal diffusivity, respectively. A constant value of specific heat, 0.68 J/(g K), was used in this work.

Table 1
Nitridation result of samples RYbM and RYM

Sample	Nitridation (%)	$\beta/(\alpha+\beta)$ (wt%)	Linear shrinkage (%)	Bulk density (g/cm^3)	Relative density (%)	Open porosity (%)
RYbM	97.8	1.7	3.6	2.67	76.4	19.5
RYM	95.9	23.4	2.7	2.39	72.7	24.0

3. Results and discussion

3.1. Nitridation of Si compacts

Table 1 gives nitridation result of samples RYbM and RYM. It is found that sample RYbM shows a slightly higher extent of nitridation than sample RYM. Sample RYbM shows slightly higher density and lower open porosity than sample RYM and this is due to the higher densification in the former than in the latter during nitridation. However, the most significant difference between samples RYM and RYbM is that the former exhibits $\beta/(\alpha+\beta)$ ratio as high as 23.4 wt%, while the latter exhibits $\beta/(\alpha+\beta)$ ratio as low as 1.7 wt%. Fig. 1 gives XRD patterns of nitrided samples RYbM and RYM. No Si peaks are observed in both the XRD patterns and this means that the nitriding reaction is completed. Because of the very low $\beta/(\alpha+\beta)$ ratio, the intensities of β-Si_3N_4 peaks are very weak in sample RYbM. In contrast, the intensities of β-Si_3N_4 peaks are strong due to the high $\beta/(\alpha+\beta)$ ratio in sample RYM. The previous paper reported that the sample RYM exhibited a $\beta/(\alpha+\beta)$ ratio of 12.6 wt%, while the RYbM a $\beta/(\alpha+\beta)$ ratio of 1.7 wt% at 1350 °C for 8 h.[8] It seems that the sample RYM shows a significant increase in the $\beta/(\alpha+\beta)$ ratio with increasing temperature from 1350 to 1400 °C, while the sample RYbM remains almost constant. This indicates that the additive composition indeed plays a key role in the $\beta/(\alpha+\beta)$ ratio of the Si_3N_4 products.

A distinct feature of the nitridation of Si is that both α- and β-phases are always simultaneously formed, that is, the Si_3N_4 products always consist of both α- and β-phases. To date, two fundamental theories have been proposed to explain the formation mechanisms of α- and β-phases. One is the theory proposed by Moulson[11] that the major growth of β-phase occurs in the liquid phase and, to a minor extent, as a result of the reaction between solid silicon and nitrogen, and the growth of α-phase occurs by vapour-phase reactions. The other is the theory proposed by Jennings[12] that the α-phase results from the reaction between silicon and molecular nitrogen and the β-phase results from the reaction between silicon and atomic nitrogen. A typical experimental example supporting Moulson' theory is that the incorporation of iron impurity promotes the formation of β-phase due to the presence of a liquid phase (often $FeSi_2$). However, Jennings's theory suggested that the β-phase does not necessarily require a liquid phase, although it is indeed favoured by its presence. Pigeon et al.[13] conducted a series of experiments to provide evidence for Jennings's theory.

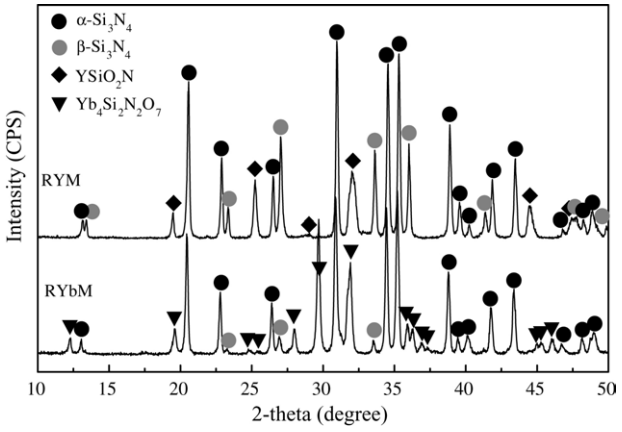

Fig. 1. XRD patterns of nitrided samples RYbM and RYM.

In the present work, the sintering additives were used to exert twofold functions. One is to accelerate the nitridation reaction by removing SiO_2 layer on the Si particles and forming a liquid phase. The other is to promote the densification of RBSN bodies during post-sintering by providing a liquid-phase sintering mechanism. XRD patterns of nitrided samples presented in Fig. 1 reveal that the crystalline secondary phases are formed during nitridation. The $Yb_4Si_2O_7N_2$ phase is observed in sample RYbM and the $YSiO_2N$ phase is observed in sample RYM. The formation of these crystalline secondary phases was observed at 1150 °C and this was in accordance with findings of Kleebe et al.[14] The formation of these crystalline secondary phases is attributed to the chemical reaction between rare-earth oxides, SiO_2 on the surface of Si particles and Si or newly formed Si_3N_4 during nitridation. However, no crystalline secondary phases containing Mg were detected by XRD. It has been reported that the lowest eutectic temperature of the Si_3N_4–SiO_2–Yb_2O_3–MgO is near 1350 °C.[15] It can be believed that the lowest eutectic temperature of the Si_3N_4–SiO_2–Y_2O_3–MgO does not exceed 1350 °C. The results suggest that the Y_2O_3 and Yb_2O_3 additives are mainly active in removing the SiO_2 layer on the surface of Si particles, while the MgO additive takes part in the formation of a liquid phase, both promoting the nitridation. The increase in temperature from 1350 to 1400 °C should lead to an increase in the amount of liquid phase in both samples RYbM and RYM. Furthermore, since the nitriding reaction is highly exothermic, the melting of some Si particles should occur due to the local temperature over the melting point of Si (1410 °C) at the nitriding temperature of 1400 °C. However, the samples RYbM nitrided at this temperature does not exhibits any change in the $\beta/(\alpha+\beta)$ ratio, compared with those nitrided at 1350 °C. This contradicts with the theory proposed by Moulson, but it seems to

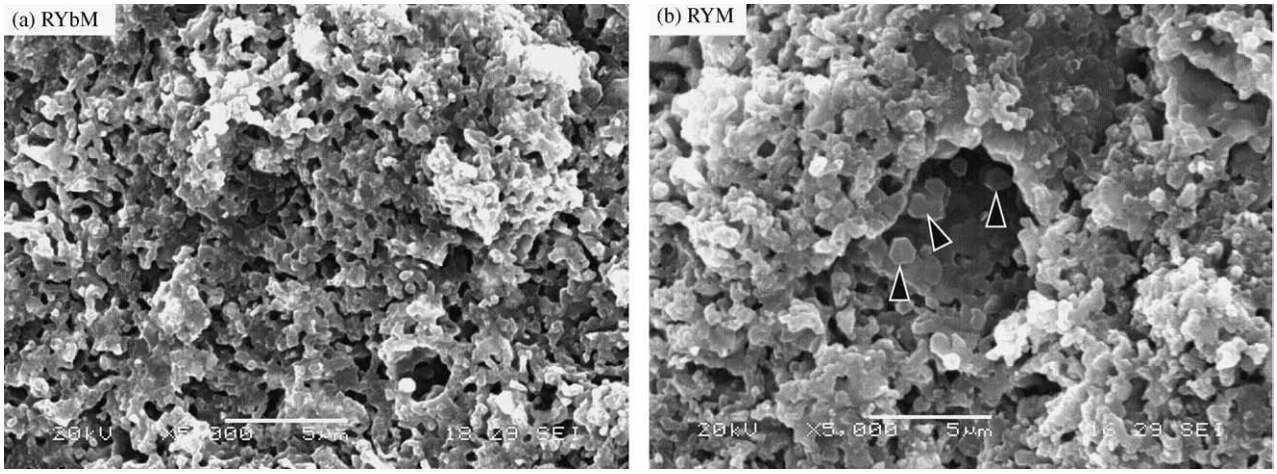

Fig. 2. SEM micrographs of the fracture surfaces of the nitrided samples: (a) RYbM and (b) RYM (5000× magnification, bar = 5 μm).

be in agreement with the theory proposed by Jennings. As a result, the significant difference in the $\beta/(\alpha+\beta)$ ratio between samples RYbM and RYM is likely that the YM additive composition promotes the formation of atomic nitrogen, while the YbM additive composition inhibits the formation of atomic nitrogen during nitridation.

Fig. 2 shows SEM micrographs of fracture surfaces of nitrided samples. The samples RYbM and RYM both exhibit a typically microstructural development of RBSN—porous microstructure. In both cases, most of the Si_3N_4 grains are fine and equiaxed in an agglomerated form. However, there is a distinct difference in the microstructure between the samples RYbM and RYM. As indicated by arrowheads in Fig. 2(b), a few rodlike β-Si_3N_4 grains with large size are formed in the sample RYM, but such "unique" grains are not observed in the sample RYbM. This distinct difference will exert a marked effect on their microstructual evolution during post-densification. This effect will be discussed in the next section.

3.2. Sintering, secondary phases and microstructure

Table 2 gives linear shrinkages, weight loss and densities of sintered RBSN (SRBSN) and sintered Si_3N_4 (SSN). It is found that the samples RYM and SYM both are densified to more than 99% relative density, indicating that the processing method has no effect on the densification of Si_3N_4 with the YM additive composition. However, when the YbM composition is used as sintering additives, the processing method has an effect on the densification of Si_3N_4. The sample SYbM arising from raw Si_3N_4 powder is densified to nearly 99% relative density, but the sample RYbM arising from reaction-bonding of raw Si powder is densified to less than 95% relative density. It is evident that the SRBSN (RYbM and RYM) materials exhibit substantially smaller sintering shrinkages than the SSN (SYbM and SYM) materials, because the RBSN bodies (>70% relative density) have significantly higher densities than the Si_3N_4-powder green bodies (∼53% relative density). Due to the incomplete densification (∼95% relative density) and higher starting density, the sintering shrinkage of sample RYbM is smaller than that of sample RYM. It is very interesting to see that the samples RYbM and SYbM both exhibit weight loss of ∼6 wt%, but the samples RYM and SYM both exhibit weight loss of ∼2 wt%. This appears to indicate that the weight loss of Si_3N_4 during sintering is not affected by the processing method.

Fig. 3 gives XRD patterns of sintered RBSN and sintered Si_3N_4 materials. It is shown that the α- to β-phase transformation has been completed in all cases during sintering. The $Yb_4Si_2O_7N_2$ phase is observed in both the samples SYbM and RYbM, and the $Y_2Si_3O_3N_4$ phase is observed in both the samples SYM and RYM. As a result, compared with the crystalline secondary phase formed during nitridation, the sample RYM exhibits the change of crystalline secondary phase from $YSiO_2N$ to $Y_2Si_3O_3N_4$, but the sample RYbM still exhibits the same crystalline secondary phase $Yb_4Si_2O_7N_2$ after sintering.

Fig. 4 presents low magnification SEM micrographs of sintered RBSN and sintered Si_3N_4 materials. Due to incomplete densification, a number of large pores are present in

Table 2
Linear shrinkage, weight loss, density, thermal diffusivity and thermal conductivity for sintered RBSN (SRBSN) and sintered Si_3N_4 (SSN) materials

Sample number	Linear shrinkage (%)	Weight loss (%)	Bulk density (g/cm^3)	Relative density (%)	Thermal diffusivity ($cm^2\ s^{-1}$)	Thermal conductivity ($Wm^{-1}\ K^{-1}$)
RYbM	8.8	6.6	3.32	94.7	0.412	93
RYM	11.3	2.4	3.26	99.1	0.387	86
SYbM	18.9	5.5	3.46	99.0	0.387	91
SYM	19.1	2.3	3.27	99.4	0.382	85

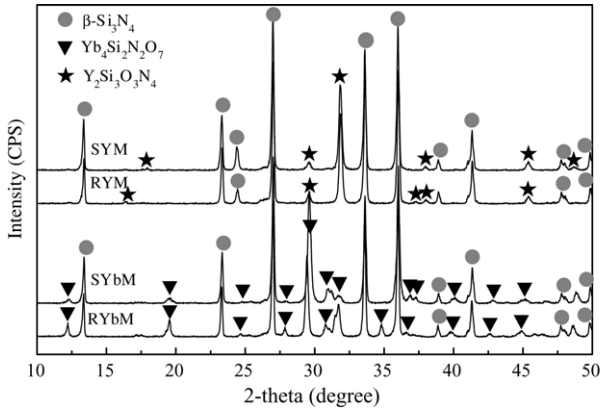

Fig. 3. XRD patterns of sintered RBSN (RYbM and RYM) and sintered Si_3N_4 (SYbM and SYM).

the sample RYbM. However, few pores are observed in other samples due to nearly complete densification. All materials exhibit a similar microstructure composed of fine matrix grains and large elongated grains. Fig. 5 also presents high magnification SEM micrographs of sintered RBSN and sintered Si_3N_4 materials. It is clear that the sample SYbM exhibits almost the same microstructure as the sample SYM, but the sample RYbM exhibits coarser microstructure than the sample RYM. It is very interesting to see that a few large elongated β-Si_3N_4 grains with exceptionally high aspect ratio are observed in only the sample RYM and they reach lengths of even up to 150 μm, as shown by arrowhead in Fig. 4(b). This implies that the exaggerated growth of elongated β-Si_3N_4 grains occurs in only the sample RYM, resulting in a highly bimodal microstructure. It is also noted that the sample RYbM contains lower amount of secondary phases than the sample RYM. The decreased amount of secondary phase is likely responsible for the poor post-densification behaviour of the nitrided RYbM. It has been shown that the nearly complete densification of RBSN bodies with the YbM additive composition could be achieved by adding Si_3N_4 powder to green bodies or lowering nitriding temperature, suggesting that the agglomerates formed in RBSN could likely hinder the post-densification in that paper.[15] Although the nitrided RYM also exhibits agglomerated microstructure, similar to that of the nitrided RYbM, the higher amount of secondary phase allows the former to achieve the complete densification during post-sintering. In addition, it is easily found that the

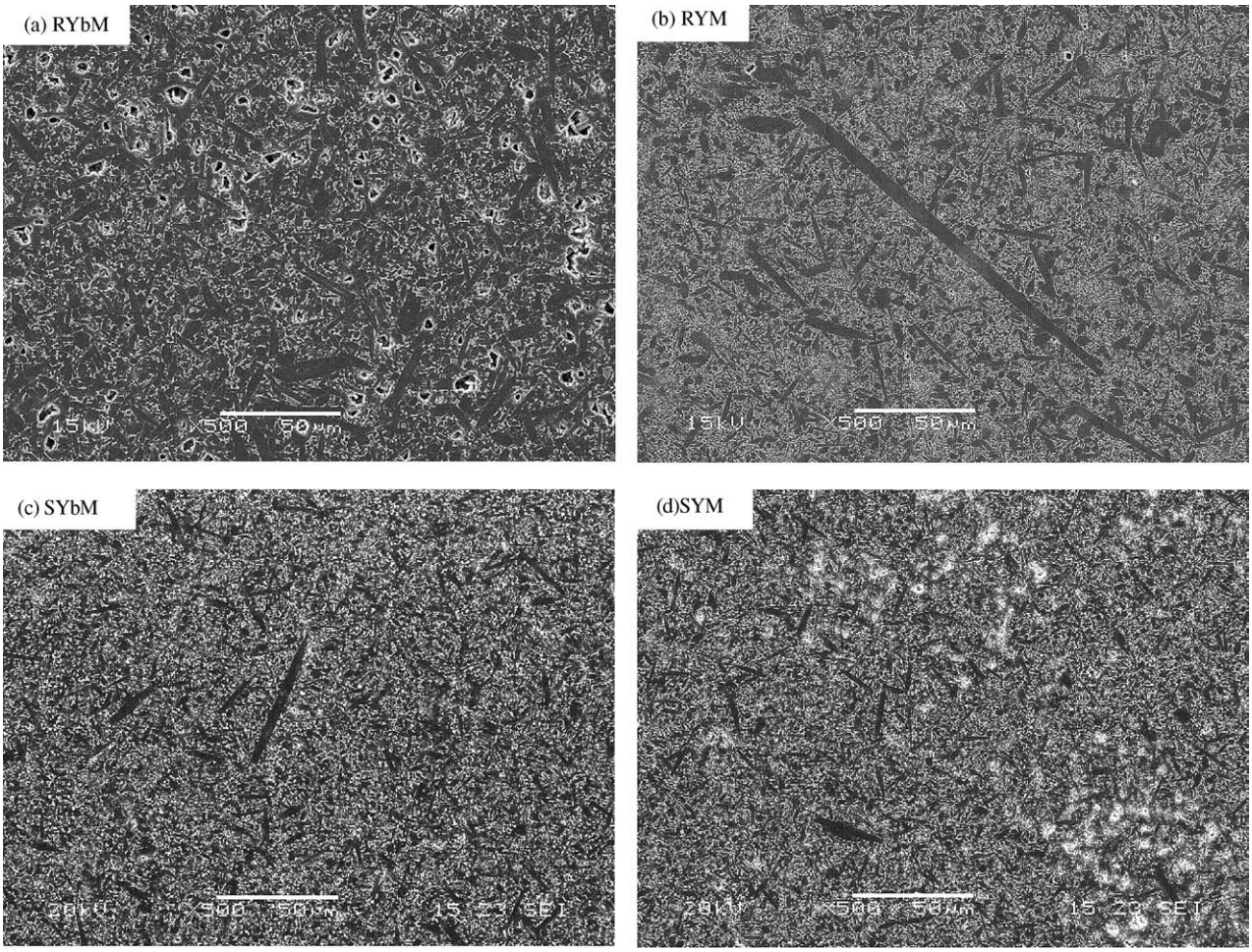

Fig. 4. Low magnification SEM micrographs of sintered RBSN: (a) RYbM and (b) RYM, and sintered Si_3N_4: (c) SYbM and (d) SYM (500× magnification, bar = 50 μm).

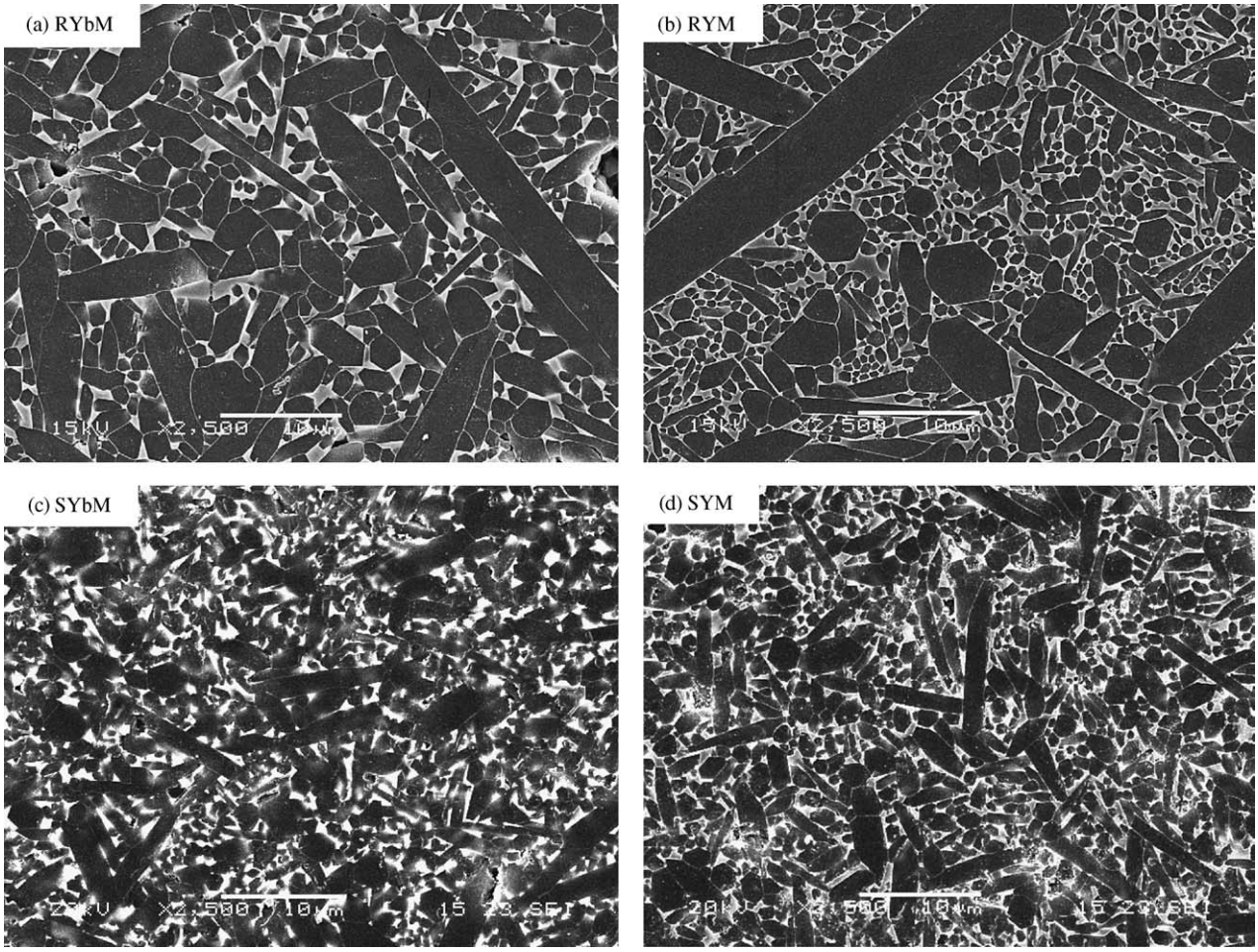

Fig. 5. High magnification SEM micrographs of sintered RBSN: (a) RYbM and (b) RYM, and sintered Si_3N_4: (c) SYbM and (d) SYM (2500× magnification, bar = 10 μm).

sample RYbM exhibits substantially coarser microstructure than sample SYbM. Compared with the sample SYM, the sample RYM exhibits a highly bimodal microstructure.

Because the densification, phase transformation and Ostwald ripening of Si_3N_4 proceed via solution-reprecipitation through the liquid phase, the microstructure and properties stongly depend on the sintering additives. It is expected that Si_3N_4 grain growth is dominated by diffusion-controlled mechanism of Ostwald ripening.[16] The similar microstructure between the samples SYbM and SYM suggests that there is no significant difference in the viscosity of the liquid phase between the Si_3N_4–Y_2O_3–SiO_2–MgO and Si_3N_4–Yb_2O_3–SiO_2–MgO systems, because the Y^{3+} ion has similar cationic field strength to the Yb^{3+} ion.[17] Thus, the difference in the microstructure between the sintered RYbM and RYM is related to the difference in the characteristics between the nitrided RYbM and RYM, developing during nitriding process.

It is well known that tough Si_3N_4 ceramic is attributed to its unique bimodal microstructure, which have abnormally grown elongated grains in the fine matrices. The abnormal grain growth in Si_3N_4 strongly depends on the amount and grain size of β-Si_3N_4 nuclei.[18,19] If the particle-size difference between large β-Si_3N_4 nuclei and fine matrix grain exceeds a critical value, the abnormal grain growth occurs by dissolution of fine grains and growth of large β-Si_3N_4 nuclei. Nevertheless, once the amount of large-nuclei exceeds a critical value, the normal grain growth instead of abnormal grain growth occurs due to the effect of steric hindrance. Using fine β-Si_3N_4 powders as raw materials, Emoto et al.[19] reported that when 0.1–10 wt% large β nuclei were added, a bimodal microstructure developed, while when 30 wt% β nuclei were added, a unimodal microstructure developed. Although the nitrided RYM contains more β-Si_3N_4 nuclei than the nitrided RYbM, there is a broader particle-size distribution for those β nuclei in the former. As shown by arrowheads in Fig. 2(b), these large β nuclei grow very fast by consuming adjacent small grains during sintering, resulting in a highly bimodal microstructure. Therefore, compared with the sample RYbM, the reason why the sample RYM exhibits exaggerated grain growth during sintering is probably due to the presence of large rodlike β-Si_3N_4 grains in the nitrided body.

3.3. Thermal conductivity

Table 2 also gives thermal diffusivities and thermal conductivities of sintered RBSN and sintered Si_3N_4. It is found that the sample SYbM shows the same thermal diffusivity as the sample SYM, but the higher density leads to higher thermal conductivity value of the former, because thermal conductivity is a function of density in terms of the Eq. (1). It has been demonstrated that the thermal conductivity of β-Si_3N_4 at room temperature is basically governed by the dissolved oxygen in the lattice of Si_3N_4, which causes phonon-defect scattering, thereby lowering thermal conductivity. The removal of lattice oxygen could be achieved by using sintering additives that react with SiO_2 and form stable compounds, thus thermal conductivity could be enhanced.[4,20] In addition, some microstructural factors affect the thermal conductivity, such as grain size, secondary phase (amount and location), grain boundary film thickness, Si_3N_4–Si_3N_4 contiguity.[21] The same thermal diffusivity between the samples SYbM and SYM is attributed to not only the similar abilities of removing lattice oxygen between Y_2O_3 and Yb_2O_3,[16] but also the similar microstructure between them.[4,21]

It is very interesting to see that despite incomplete densification, the sample RYbM shows higher thermal diffusivity/conductivity than the sample RYM. Although several studies demonstrated both theoretically and experimentally that the only grain growth could not improve thermal conductivity of Si_3N_4 ceramics,[21,22] the grain growth accompanies the removal of lattice oxygen via dissolution–reprecipitation process through the liquid phase. In such a case, smaller impure grains with a higher concentration of oxygen can dissolve in the liquid and precipitate as purer Si_3N_4 on larger β-Si_3N_4 grains. The purification of the precipitated β-Si_3N_4 grains leads to the enhancement in the thermal conductivity. Many studies have shown that the thermal conductivity of β-Si_3N_4 ceramics indeed increases with increasing amount of purified large grains.[23,24] Therefore, one reason why sample RYbM shows higher thermal diffusivity/conductivity than sample RYM is related to the larger overall grain size. Also, Si_3N_4 ceramics is actually a multiphase system consisting of Si_3N_4 grains and secondary phases. The secondary phases lower thermal conductivity because they have very low thermal conductivity, say, as low as 1 $Wm^{-1}K^{-1}$, much lower than that of the Si_3N_4 grains (∼320 $Wm^{-1}K^{-1}$).[4] The thermal conductivity decreases with increasing amount of secondary phases. Furthermore, the effect of the secondary phases on thermal conductivity strongly depends on their distribution: a continuous distribution around the matrix grains greatly lowers thermal conductivity, but an isolated distribution does not significantly affect thermal conductivity.[25,26] As shown in Fig. 5(a) and (b), the striking differences can be viewed in the microstructure between samples RYbM and RYM: (1) sample RYbM shows lower amount of secondary phases and larger overall grain size than sample RYM and (2) the secondary phases in sample RYbM are almost located in isolated pockets at the triple grain boundary junctions and this results in higher Si_3N_4–Si_3N_4 contiguity, while a large amount of small grains in sample RYM is surrounded by the secondary phases and this results in a lower Si_3N_4–Si_3N_4 contiguity. Therefore, the other reason why the sample RYbM shows higher thermal diffusivity/conductivity than the sample RYM is attributed to the lower amount of secondary phases and higher Si_3N_4–Si_3N_4 contiguity.

As discussed above, these results show that the replacement of Yb_2O_3 by Y_2O_3 has no significant effect on the thermal conductivity of SSN materials, but it has an effect on the thermal conductivity of SRBSN materials. More importantly, the present work implies that SRBSN materials with comparable or even superior thermal conductivity to SSN materials could be achieved.

4. Conclusions

Both sintered reaction-bonded silicon nitride (SRBSN) and sintered Si_3N_4 (SSN) materials were fabricated by gas-pressure sintering at 1900 °C for 6 h under a nitrogen pressure of 1 MPa, using two additive compositions of Yb_2O_3–MgO (YbM) and Y_2O_3–MgO (YM). The effect of additive composition on the microstructure and thermal conductivity of Si_3N_4 ceramics was found to strongly depend on the processing method. The SSN materials with YbM exhibit the same full density, microstructure and thermal diffusivity as those with YM. The same microstructure is probably due to the fact that there is no significant difference in the viscosity of the liquid phase between the Si_3N_4–Y_2O_3–SiO_2–MgO and Si_3N_4–Yb_2O_3–SiO_2–MgO systems. However, the replacement of Yb_2O_3 by Y_2O_3 has a strong effect on the processing, microstructure and thermal conductivity of SRBSN. During nitridation, the YM additives promote the formation of β-Si_3N_4 and even the formation of large rodlike β-Si_3N_4, but the YbM additives retard the formation of β-Si_3N_4. During post-sintering, the SRBSN materials with YM exhibit nearly full densification and highly bimodal microstructure, but those with YbM exhibit incomplete densification and an overall coarse microstructure. The reason why the YM additive leads to highly bimodal microstructure is probably attributed to the presence of large rodlike β-nuclei in the nitrided bodies. Despite the incomplete densification, the SRBSN materials with YbM exhibit higher thermal conductivity than those with YM and this is due to the lower amount of secondary phase, larger overall grain size and higher Si_3N_4–Si_3N_4 contiguity in the former.

References

1. Riley, F. L., Silicon nitride and related materials. *J. Am. Ceram. Soc.*, 2000, **83**(2), 245–265.
2. Haggerty, J. S. and Lightfood, A., Opportunities for enhancing the thermal conductivity of SiC and Si_3N_4 ceramics through improved processing. *Ceram. Eng. Sci. Proc.*, 1995, **16**(4), 475–487.

3. Hirosaki, N. S., Kocer, O., Kitagawa, C. H. and Nakamura, Y., Molecular dynamics calculation of the ideal thermal conductivity of single-crystal α- and β-Si_3N_4. *Phys. Rev. B*, 2002, **65**, 134110.
4. Hirao, K., Watari, K., Hayashi, K. H. and Kitayama, M., High thermal conductivity silicon nitride. *MRS Bull.*, 2001, **26**(6), 451–455.
5. Ziegler, G., Heinrich, J. and Wötting, G., Relationships between processing, microstructure, and properties of dense and reaction-bonded silicon nitride. *J. Mater. Sci.*, 1987, **22**, 3041–3086.
6. Lee, B. T., Yoo, J. H. and Kim, H. D., Microstructure characterization of GPSed-RBSN and GPSed-Si_3N_4 ceramics. *Mater. Trans., JIM*, 2000, **41**(2), 312–316.
7. Lee, J. S., Mun, J. H., Han, B. D. and Kim, H. D., Effect of β-Si_3N_4 seed particles on the property of sintered reaction-bonded silicon nitride. *Ceram. Int.*, 2003, **29**, 897–905.
8. Zhu, X. W., Zhou, Y. and Hirao, K., Effect of sintering additive composition on the processing and thermal conductivity of sintered reaction-bonded Si_3N_4. *J. Am. Ceram. Soc.*, 2004, **87**(7), 1398–1400.
9. Zhu, X. W., Zhou, Y. and Hirao, K., Development of sintered reaction-bonded Si_3N_4 with high thermal conductivity. *J. Ceram. Soc. Jpn., Suppl.*, 2004, **112**(5), S410–S414.
10. Pigeon, R. G. and Varma, A., Quantitative phase analysis of Si_3N_4 by X-ray diffraction. *J. Mater. Sci. Lett.*, 1992, **11**, 1370–1372.
11. Moulson, A. J., Reaction-bonded silicon nitride: its formation and properties. *J. Mater. Sci.*, 1979, **14**, 1017–1051.
12. Jennings, H. M., On reactions between silicon and nitrogen. Part 1. Mechanisms. *J. Mater. Sci.*, 1983, **18**, 951–967.
13. Pigeon, R. G., Varma, A. and Miller, A. E., Some factors influencing the formation of reaction-bonded silicon nitride. *J. Mater. Sci.*, 1993, **28**, 1919–1936.
14. Kleebe, H. J. and Ziegler, G., Influlence of crystalline secondary phases on the densification behavior of reacion-bonded silicon nitride during postsintering under increased nitrogen pressure. *J. Am. Ceram. Soc.*, 1989, **72**(12), 2314–2317.
15. Zhu, X. W., Zhou, Y. and Hirao, K., Post-densification behaviour of reaction-bonded silicon nitride (RBSN): effects of various characteristics of RBSN. *J. Mater. Sci.*, 2004, **39**, 5785–5797.
16. Kitayama, M., Hirao, K., Watari, K., Toriyama, M. and Kanzaki, S., Thermal conductivity of β-Si_3N_4. III. Effect of rare-earth (RE = La, Nd, Gd, Y, Yb, and Sc) oxide additives. *J. Am. Ceram. Soc.*, 2001, **84**(2), 353–358.
17. Ramesh, R., Nestor, E., Pomeroy, M. J. and Hampshire, S., Formation of Ln–Si–Al–O–N glasses and their properties. *J. Eur. Ceram. Soc.*, 1997, **17**, 1933–1939.
18. Dressler, W., Kleebe, H. J., Hoffmann, M. J., Rühle, M. and Petzow, G., Model experiments concerning abnormal grain growth in silicon nitride. *J. Eur. Ceram. Soc.*, 1996, **16**, 3–14.
19. Emoto, H. and Mitomo, M., Control and characterization of abnormally grown grains in silicon nitride ceramics. *J. Eur. Ceram. Soc.*, 1997, **17**, 797–804.
20. Kitayama, M., Hirao, K., Tsuge, A., Watari, K., Toriyama, M. and Kanzaki, S., Thermal conductivity of β-Si_3N_4. II. Effect of lattice oxygen. *J. Am. Ceram. Soc.*, 2000, **83**(8), 1985–1992.
21. Kitayama, M., Hirao, K., Toriyama, M. and Kanzaki, S., Thermal conductivity of β-Si_3N_4. I. Effect of various microstructural factors. *J. Am. Ceram. Soc.*, 1999, **82**(11), 3105–3112.
22. Watari, K., Hirao, K., Toriyama, M. and Ishizaki, K., Effect of grain size on the thermal conductivity of Si_3N_4. *J. Am. Ceram. Soc.*, 1999, **82**(3), 777–779.
23. Yokota, H., Abe, H. and Ibukiyama, M., Effect of large β-Si_3N_4 particles on the thermal conductivity of β-Si_3N_4 ceramics. *J. Eur. Ceram. Soc.*, 2003, **23**, 1175–1182.
24. Yokota, H. and Ibukiyama, M., Effect of the addition of β-Si_3N_4 nuclei on the thermal conductivity of β-Si_3N_4 ceramics. *J. Eur. Ceram. Soc.*, 2003, **23**, 1183–1191.
25. Kim, W. J., Kim, D. Y. and Kim, C. H., Morphological effect of second phase on the thermal conductivity of AlN ceramics. *J. Am. Ceram. Soc.*, 1996, **79**(4), 1066–1072.
26. Boey, F., Tok, A. I. Y. Y., Lam, C. and Chew, S. Y., On the effects of secondary phase on thermal conductivity of AlN ceramic substrates using a microstructural modelling approach. *Mater. Sci. Eng. A*, 2002, **335**, 281–289.